

Stable boundary layer vertical scales in the Arctic: observations and analyses at Ny-Ålesund, Svalbard

M. Mazzola,^{a*} F. Tampieri,^a A.P. Viola,^b C. Lanconelli,^a and T. Choi^c

^aNational Research Council of Italy, Institute of Atmospheric Sciences and Climate (CNR-ISAC), Bologna, Italy

^bNational Research Council of Italy, Institute of Atmospheric Sciences and Climate (CNR-ISAC), Roma, Italy

^cKorea Polar Research Institute (KOPRI), Incheon, Korea

*Correspondence to: M. Mazzola, Institute of Atmospheric Science and Climate, CNR, Via Gobetti 101, 40129, Bologna, Italy.
E-mail: m.mazzola@isac.cnr.it

An extensive set of measurements (May–August 2012 and June–November 2013) taken at the Amundsen-Nobile Climate Change Tower located at Ny-Ålesund, Svalbard, allowed investigation of some features of the vertical structure of the atmospheric stable boundary layer (SBL) at high latitudes. The main sensors are three sonic anemometers and four low-frequency thermo-hygrometers and anemometers. The momentum flux τ , the sensible heat flux Q and the turbulent kinetic energy K data at different levels demonstrated the occurrence of both the traditional and upside-down SBL cases, according to the classification proposed in the literature. Based on a linear approximation of the profiles, the vertical scales were found to be different for the different second-order moments. In the traditional case, the scales h_τ , h_Q and h_K , defined as levels for which fluxes became zero, can be considered to approximate the boundary-layer depth. While the distributions of h_τ and h_Q were found to be similar, having the ratio h_Q/h_τ equally distributed around unity although with a positive skewness, those of h_τ and h_K look quite different, having the ratio $h_K/h_\tau > 1$ in about 90% of the cases and with a median value > 2 . In the upside-down case, the scales s_τ , s_Q and s_K , defined as the height at which the value of the considered quantity doubles that at the surface, give a measure of the vertical variations of the moments. Comparing the distributions of these three scales, similar results to those for the traditional case were found, although with slightly different statistics. The values of the ratio between scales affect the vertical profile of the local Obukhov length in both the traditional and upside-down SBL cases.

Key Words: stable boundary layer; SBL vertical scales; arctic boundary layer; Svalbard

Received 17 December 2014; Revised 11 November 2015; Accepted 15 December 2015; Published online in Wiley Online Library 9 February 2016

1. Introduction

The Arctic areas are subject to global warming more than other regions on Earth, while the loss of sea ice is faster than predicted by most of the climate models. The feedback mechanisms from loss of sea ice and changes in atmospheric and oceanic circulations contribute to the so-called Arctic amplification Stroeve *et al.*, 2007, 2012; Serreze *et al.*, 2009. The IPCC AR5 report (IPCC, 2013) pointed to unprecedented changes in the global environment and noted several pieces of evidence supporting the Arctic warming. In particular, changes observed over the past 2–3 years are even beyond the most pessimistic of the model predictions used in the IPCC AR4 report (IPCC, 2007). Therefore the complexity of the climate system requires deeper knowledge of the processes that determine climate variability in the Arctic region and of their representation in meteorological and climatological models. Improvements are

required in theoretical understanding to improve the accuracy of models at high latitudes, as well as the interpretation of long time series of different parameters. The atmospheric boundary layer (ABL) is one of the elements in the climate system that needs to be tuned from both point of views. Knowledge of the ABL is essential to obtain a quantitative understanding of the exchange processes between the Earth's surface and the lowest atmospheric layers and to test the parametrization schemes to be used in numerical weather prediction, atmospheric composition and climate models. In this context, high-quality observations of the polar ABL are necessary to improve our knowledge of turbulence under conditions which can be very different from those typically occurring in midlatitudes, for instance due to the small amplitude (or even the absence) of the diurnal cycle of solar forcing.

A few datasets collected in polar sites with these features are available: for instance, in the frame of the Surface Heat Budget of the Arctic Ocean experiment (SHEBA; Andreas *et al.*, 1999;

Persson *et al.*, 2002) a 20 m tower with five sonic anemometers was deployed for almost one year on Arctic sea ice. Handorf *et al.* (1999) analyzed a four-year dataset of profile measurements up to 45 m height and a one-month dataset of turbulence measurements up to 11 m from the German Neumayer Station in Antarctica in order to assess closure schemes for the ABL.

The Svalbard archipelago is located at the northern margin of the warm sea current coming from the lower latitudes of the Atlantic Ocean and lies in an ideal position to monitor the combined effects of climate change affecting the atmosphere, as well as the ocean and land. Kilpeläinen and Sjöblom (2010) and Kral *et al.* (2014) analyzed marine boundary-layer data from tower measurements taken in the ice-free Isfjorden over the period 2008–2010. Maturilli *et al.* (2013) presented a consistent meteorological dataset collected at Ny-Ålesund from 1993 to 2011 but, even though these data provide a good picture of the climatological variation of the atmospheric variables in the area, they are not sufficient to describe the vertical structure of the ABL. Jocher *et al.* (2015) compared one year of sensible heat flux eddy covariance measurements performed at Ny-Ålesund with corresponding model results. In order to extend the availability of this kind of measurement, a 34 m high tower was set up at Ny-Ålesund, Svalbard in 2009 by the National Research Council of Italy (CNR).

The characterization of Stable Boundary Layers (SBLs) is a challenging task and different approaches exist, depending on which aspects are examined. According to Sun *et al.* (2012) and Monahan *et al.* (2015), SBL regimes are characterized by parameters such as a measure of stability (Obukhov length and Richardson number), the velocity at different levels and the potential temperature gradients. Mahrt and Vickers (2002) characterized the SBL by means of the vertical variations of some second-order moments, suggesting a distinction between the traditional SBL and the upside-down SBL. Broadly speaking, traditional SBLs are affected by surface values of the momentum flux and the absolute value of heat flux, which decrease with height. The SBL depth can be defined as the height at which these fluxes become negligible. They have been subject of many investigations using observations (e.g. Caughey *et al.*, 1979; Grachev *et al.*, 2005) and models (recently reviewed in Bosveld *et al.*, 2014). Upside-down SBLs are characterized by the production of turbulence aloft (Banta *et al.*, 2006; Mahrt, 2014), so that both turbulent kinetic energy and momentum flux increase with height. The absolute values of momentum and heat fluxes near the ground can be very small, so that in general they are not representative of the turbulence structure of the entire SBL. The stability (measured by the Richardson number) is expected to increase with height, with associated production of gravity waves (Sorbján and Czerwinska, 2013). Large shear below the low-level jet may also enhance turbulence production. In the literature, the depth of the upside-down SBL is usually identified with the height of the maximum velocity of the low-level jet.

The purpose of this article is to identify and discuss the vertical structure of SBL in terms of turbulence profiles, using the dataset obtained from the Amundsen-Nobile Climate Change Tower. In section 2 the experimental set-up is described. In section 3 the vertical profiles of momentum and heat fluxes and of turbulent kinetic energy for traditional and upside-down SBLs are analyzed and suitable scale heights are derived. In section 4 the implications of the vertical variations of the fluxes on the stability evaluated at different heights are discussed. In section 5 some conclusions are drawn and further questions are posed.

2. Measurement site and dataset

The Department of Earth System Science and Environmental Technologies of CNR has recently financed the construction of the Amundsen-Nobile Climate Change Tower (CCT). The tower was installed at the end of 2009 about 2 km northwest of the village of Ny-Ålesund (78°55'N, 11°52'E) on the southern coast

Table 1. List of measuring instruments used in this work.

Sensor	Height (m)	Acquisition rate
Vaisala HMP45AC thermo-hygrometer	2.0, 4.8, 10.3, 33.4	1 min
Young Marine Wind Monitor 05106 anemometer	2.0, 4.8, 10.3, 33.4	1 min
Gill R2 sonic anemometer (R2)	3.7	21 Hz
Gill R3 sonic anemometer (R3)	7.5	20 Hz
Campbell Scientific CSAT3A (CS)	21.0	10 Hz

of Kongsfjorden, on the archipelago of Svalbard (Norway), within the framework of the so-called Climate Change Tower Integrated Project (CCT-IP; <http://www.isac.cnr.it/~radiclim/CCTower/>; accessed 31 December 2015). The fjord is oriented south-east–northwest, is bounded by hills, steep mountains and glaciers and to the northwest is open to the ocean. The orography of the area is quite complex because within a few metres the landscape changes from the sea to mountains of 500–600 m height. As a result, three main wind sectors are identifiable: the first coming from the interior of the fjord, with origin from between east and southeast and with the highest speed, the second coming from a valley south of the site, with origin between south and southwest, and the third, present only during the summer, coming from the open sea, with origin from northwest.

The tower is 34 m high and is conceived to provide a scientific platform for atmospheric monitoring activities in such an orographically complex area, to complement other researches, and to host new experiments and instruments devoted to the study of processes concerning the climate system in the Arctic.

Since the beginning the tower was equipped with four thermo-hygrometers and four propeller anemometers at heights of 2.0, 4.8, 10.3 and 33.4 m, a four-component net radiometer at the top of the tower, and a couple of pyranometer-pyrgeometers installed at 25 m measuring the outgoing radiation, a sonic range sensor, an infrared camera and two PT100 resistance thermometers measuring the snow height, skin and internal temperatures, and a flux plate at the snow–ground interface. Later, other instruments were installed at CCT. During March 2010 a set consisting of a sonic anemometer (model Gill R3) and a fast hygrometer (Campbell Scientific KH2O) was installed at an height of 7.5 m, while during May 2012 two other similar sets were installed at 3.7 m (Gill R2 sonic anemometer and Campbell Scientific KH2O) and at 21 m (Campbell Scientific CSAT3 sonic anemometer, hereafter CS, and EC150 gas analyser). This last set of instruments was provided by the Korea Polar Research Institute (KOPRI), as part of a collaboration with CNR, as well as a Picarro Cavity Ring-Down Spectroscopy (CRDS) system, a LI-7700 methane analyzer and a LI-7500A carbon dioxide and water vapour analyzer, both by Licor, installed at the same time and at the same height of 21 m. The raw data are recorded continuously.

In this work we use measurements from the three sonic anemometers (here referred to imply as R2, R3 and CS; Table 1) over two time periods: 25 May–17 August 2012 and 15 June–26 November 2013 (i.e. periods with the R2, R3, CS anemometers active). The sampling rates of the three instruments are 10 Hz for CS, 20 Hz for R3 and 21 Hz for R2, while average quantities were evaluated over 10 min intervals, resulting in 28 331 cases being obtained. A fixed averaging time can introduce a bias because of non-turbulent low-frequency motions and, while such techniques as the multiresolution flux decomposition (Howell and Mahrt, 1997) could be highly recommended, we did not apply it because of the huge amount of data. Different authors used 30 min averages in analyses of this kind (e.g. Jocher *et al.*, 2015). Kilpeläinen and Sjöblom (2010) demonstrated by means of Ogive plots that a 30 min averaging period is appropriate for momentum flux, while for sensible heat flux an even a shorter period could be sufficient. In this work the interval length of

Table 2. Number of cases used in this work.

Samples	Total: 28 331		Stable: 14 294		
			Satisfying Eq. (1)	Of which:	
Traditional SBL	2 382	tSBL	689	Increasing K	237
				Decreasing K	310
				Increasing $\langle w^2 \rangle$	407
				Decreasing $\langle w^2 \rangle$	215
Upside-down SBL	4 352	uSBL	1 253	Increasing Q	585
				Decreasing Q	545
				Increasing $\langle w^2 \rangle$	1205
				Decreasing $\langle w^2 \rangle$	15
Constant-flux SBL	882	cSBL	42		

10 min was chosen as a compromise between the quality of the results and the need for good statistics.

3. The vertical structure of the SBL

For this work we have defined the stable cases as those with negative value of the kinematic heat flux $Q(z) = \langle w\theta \rangle(z)$ measured at the lowest sonic anemometer R2, where $w(z)$ and $\theta(z)$ are the fluctuations of the vertical velocity component and of the potential temperature, respectively, and the brackets stand for the averaging operation. This choice allows the possibility of observing a change in sign of the stability at the upper levels (C. Yagüe, 2015; personal communication).

As reported in Table 2, 14 294 stable cases were identified in the complete dataset (50% of all samples over the four years). Dai *et al.* (2011) found a similar SBL percentage from examining the SHEBA dataset.

It must be emphasised that in this investigation each 10 min interval (i.e. a case) is analyzed separately, thus neglecting the time evolution of the boundary layer. With this limitation in mind, the present approach must be considered as a tool to diagnose the instantaneous features of the SBL and to investigate some of the implications.

3.1. Classification of SBL

The vertical profiles of the momentum flux

$$\tau(z) = \sqrt{\langle uw \rangle^2(z) + \langle vw \rangle^2(z)},$$

the heat flux $Q(z)$, and the turbulent kinetic energy

$$K(z) = \frac{1}{2} \{ \langle u^2 \rangle(z) + \langle v^2 \rangle(z) + \langle w^2 \rangle(z) \}$$

are used to define the different types of SBL (where $u(z)$, $v(z)$ and $w(z)$ are the fluctuations of the velocity components). Hereafter, dependence of these parameters on the height z will be considered implicit, if not necessary for clarity purposes.

Different shapes of the profiles of second-order moments have been proposed in the literature as far as the traditional SBL are concerned. For example, power laws of the form $y(z) = y_0 (1 - z/h)^\gamma$, with γ ranging between 1 and 2, were suggested on theoretical and observational bases by Nieuwstadt (1984), Lenschow *et al.* (1988), and Sorbjan (1988), while Zilitinkevich and Esau (2005) recommended a Gaussian profile, based on large-eddy simulations (LESs). All the authors remark that the data scatter is large, so a unique shape cannot be chosen. To the authors' knowledge, no suggestions have been made regarding the upside-down SBL.

To investigate the shape and the variability of the profiles observed in the present dataset, the following procedure has been employed. First, the second-order moments have been linearly fitted by $y(z) = a + bz$, where y denotes τ , Q or K , using the data from the three anemometers. From the fit, the statistical errors

on the coefficients, σ_a and σ_b , and the root mean square error (RMSE) σ_y are determined. Hereafter, we refer to negative slope cases when $b < -\sigma_b$ and to positive slopes when $b > \sigma_b$, in order to ensure that the slopes are significantly different from zero. The same applies for the ground-level values a . To select cases in which the linear fit is a good approximation of the height-dependence of the moments (a linear profile), the following criterion is adopted:

$$\left| \frac{\sigma_y}{y(Z)} \right| < 0.2, \quad (1)$$

i.e. the RMSE of the data with respect to the fit must be less than 20% of a normalization value. Note that the numerical threshold (0.2) has been chosen on a purely empirical basis, and that the RMSE is normalized over the value of the appropriate variable estimated from the fit at a reference height $Z = 10$ m, intermediate among the measurement levels.

In order to characterize cases which depart from the linear ones, the observations at the two lowest sensor levels and those at the two highest ones have also been considered separately, obtaining b_1 and b_2 , i.e. the slopes of the lines connecting the values measured at R2 and R3 and R3 and CS, respectively. The scatterplot of the slopes b_1 and b_2 is shown in Figure 1 for the momentum and heat fluxes, giving some hints about the variability of the vertical profiles. As far as the momentum flux τ is concerned, the variability of b_1 turns out to be larger than that of b_2 for cases with a negative value of the slope of the three-instrument fit b . In other words, when τ shows an overall decrease with height, this decrease is more pronounced in the layer between R2 and R3. In fact, with reference to τ , the cases with $b_1 < b_2 < 0$ (concave decreasing profile) are 12% of the total number of SBL cases, and those with $b_2 < b_1 < 0$ (convex decreasing profile) are only 2% of cases. For cases with positive b , corresponding to an overall increase of τ with height, the number of occurrences of the concave profiles ($b_1 > b_2 > 0$) and of the convex profiles ($b_2 > b_1 > 0$) is more similar, equal to 16% and 10%, respectively. Note that in a large number of cases (59%), the signs of b_1 and b_2 are opposite, so that a well-defined trend cannot be found. Nevertheless, some of these cases are included in the definition of linear cases. In fact, in 53% of the cases, the data satisfy the criterion Eq. (1) (linearly decreasing or increasing profiles). The orange symbols in Figure 1(a) show that the linear profiles refer to the fraction of data with small $b_{1,2}$ slopes. As far as the heat flux is concerned, the picture is similar (Figure 1(b)), taking into account that this quantity is negative, at least near the ground. Cases with absolute value decreasing with height ($b > 0$, black dots) are distributed in 21% of concave profiles and 7% of convex ones. For cases with absolute value increasing with height ($b < 0$, grey dots), the fractions are 8% of concave profiles, 4% of convex ones. Again, 60% are mixed cases (b_1 and b_2 with different sign), while among all these cases, 43% are characterized by the linear shape. The behaviour of the turbulent kinetic energy (not shown here) is similar to that of momentum flux; noticeably, the frequency of linear profiles is quite high: 96%.

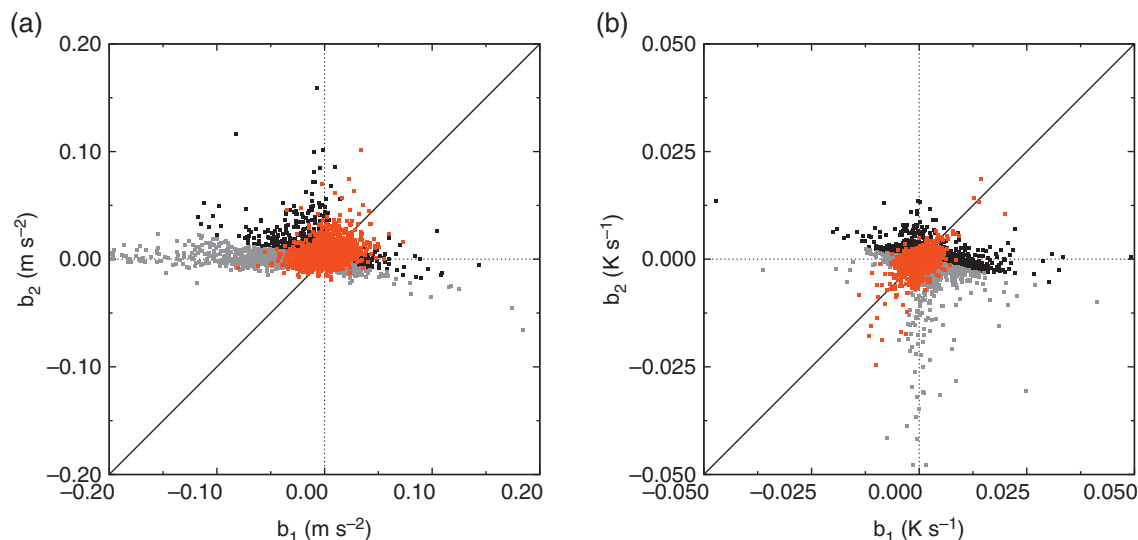


Figure 1. Scatter plot of the two-point slopes b_2 versus b_1 (for the upper and lower layer respectively; see definitions in section 3.1) for (a) momentum flux and (b) heat flux. Black symbols refer to the fitted slope $b > 0$, grey symbols to $b < 0$, and orange symbols to cases satisfying Eq. (1) (linear profiles).

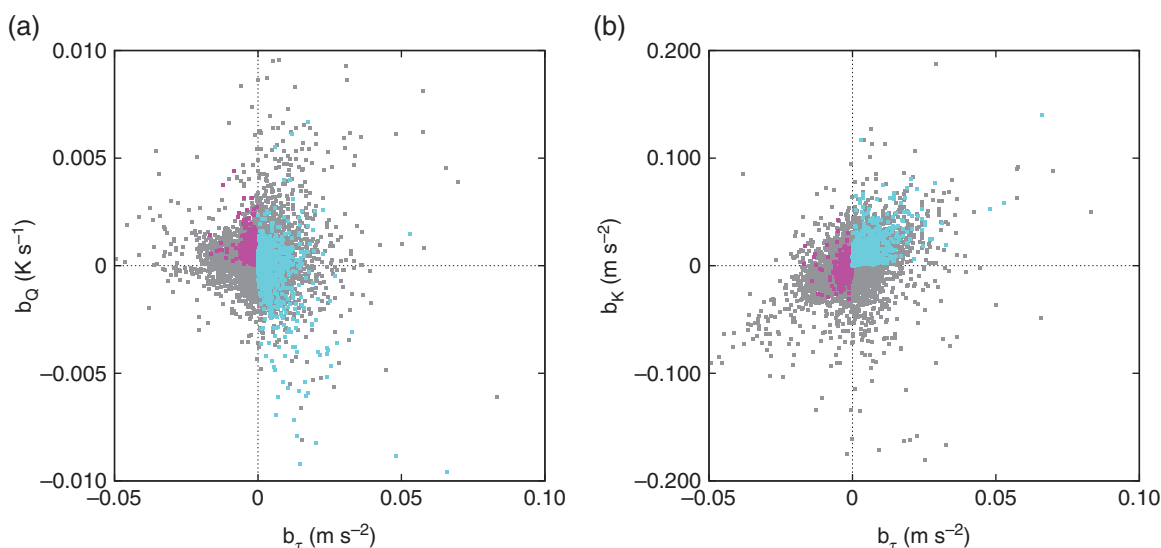


Figure 2. Scatter plot of (a) b_Q versus b_τ and (b) b_K versus b_τ for the whole SBL dataset (grey symbols), tSBL (pink symbols), and uSBL (cyan symbols).

The large profile variability displayed by the data suggests that a unique shape is not sufficient to account for all the situations, however a choice is necessary in order to classify the observations. In this article the linear profile is adopted, so that only data satisfying Eq. (1) criterion are examined.

Based on the slopes derived from the fits, we define the following SBL classes:

- tSBL is the traditional SBL case characterized by the momentum flux decreasing with height (negative $b_\tau = d\tau/dz$) and heat flux increasing with height (positive $b_Q = dQ/dz$), both satisfying the criterion (1). This results in 689 cases, equal to about one-third of the total number of cases with τ decreasing and Q increasing (Table 2). In this class about half of the cases display K decreasing with height, while about one-third display K increasing with height. Regarding the variance of the vertical velocity $\langle w^2 \rangle$, in about 60% of the cases it increases with height, and in only 30% of cases does it decrease. In about 50% of the cases, the signs of the slopes of K and $\langle w^2 \rangle$ are the same.
- uSBL is the upside-down SBL case characterized by the momentum flux and the turbulent kinetic energy increasing with height (positive b_τ and $b_K = dK/dz$). They are about one-third of the total number of cases with τ and K increasing (Table 2). In this class the cases of increasing

and decreasing Q are both about 50%. In almost all cases $\langle w^2 \rangle$ increases with height.

- An intermediate subset cSBL exists, characterized by fluxes almost constant with height and near-neutral conditions, even if it is very small (42 cases).

In the following analysis, attention is paid to tSBL and uSBL classes only, which are considered here as the two prototypical cases of the vertical structure of the SBL.

The distributions of data on the planes $(b_\tau; b_Q)$ and $(b_\tau; b_K)$ are reported in Figure 2(a) and (b), respectively. tSBL and uSBL cases are highlighted: it can be seen that in the uSBL cases the heat flux may be increasing or decreasing, while in the tSBL cases the turbulent kinetic energy may be increasing or decreasing. From Figure 2(b) it can be seen that the slopes of τ and K are often of the same sign, but a relevant number of cases occurs in which τ increases and K decreases, or vice versa. This aspect must be noticed because it means that the variances of velocity not always scale on the momentum flux; this will be discussed in the conclusions.

The influence of wind speed and direction on stability was considered. For high wind speed values (greater than 5 m s^{-1}), the tSBL and uSBL occurrences are both equal to 22%, while for values below 5 m s^{-1} , they are 13 and 36%, respectively, indicating that calm wind conditions favour the establishment of an upside-down SBL. This is confirmed by examining the sector of origin of the

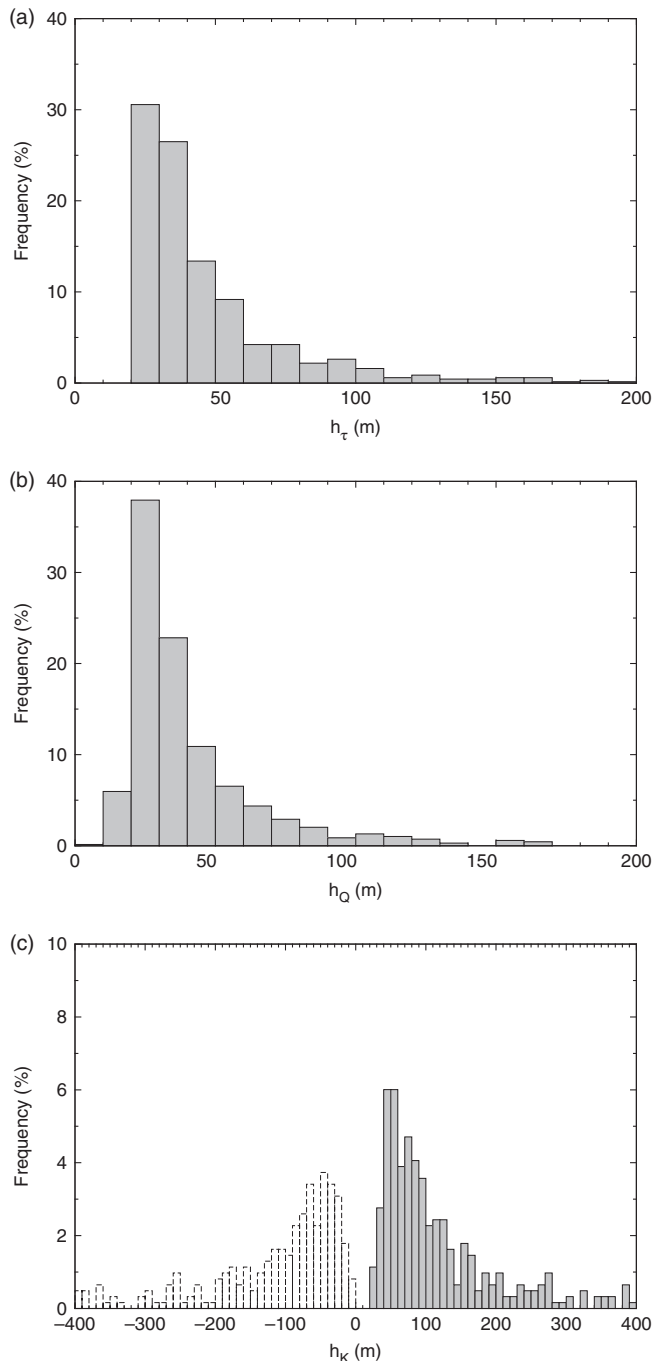


Figure 3. Frequency distributions for tSBL depths (a) h_τ , (b) h_Q , and (c) h_K .

wind: while the relative occurrences of tSBL and uSBL cases in the main east/southeast sector are similar (24 and 26%), the same values for the other two identified sectors are quite different: 12 and 32% for the wind coming from the glacier valleys, and 12 and 33% for that coming from the open sea. This because the east/southeast sector presents stronger winds than the other two sectors.

3.2. Traditional SBL

The height at which the moments become zero identifies the SBL depth. Different depth scales $h_y = -a/b$ can be derived for the momentum flux (h_τ), for the heat flux (h_Q) and for the turbulent kinetic energy (h_K) and can be considered to approximate the boundary-layer depth. The frequency distributions of the depths are reported in Figure 3. The distributions of the depths are different for the different moments, and in particular the K depth is larger than the others, i.e. K decays slower than momentum or heat fluxes. While h_τ and h_Q present similar distributions, h_K is spread much more towards higher values. The median values

Table 3. Statistics for the SBL depths in the traditional and upside-down linear cases (the 50th percentile = the median value).

	Percentiles					Average	Min	Max
	10th	25th	50th	75th	90th			
h_Q/h_τ	0.3	0.6	0.9	1.2	1.8	1.0	0.0	4.7
h_K/h_τ	0.9	1.4	2.2	3.4	5.8	3.0	0.1	18.2
h_E/h_τ	0.5	1.0	1.7	2.6	3.8	2.0	0.1	9.1
h_E/h_K	0.3	0.5	0.8	1.4	2.1	1.0	0.0	4.3
s_Q/s_τ	0.2	0.4	1.2	2.7	5.5	2.1	0.0	9.7
s_K/s_τ	0.8	1.8	4.7	12.2	26.5	10.8	0.0	99.6

are 37, 32 and 80 m respectively. As noticed above, turbulent kinetic energy decreases with height as the momentum flux does (Table 2) in 45% of the cases, but cases also occur of K being almost constant or increasing with height. Note that if τ and K would go to zero at the same height, their ratio would be constant and equal to the surface value, as predicted by the model by Nieuwstadt (1984), which is based on the assumption that the Richardson number is constant. The observation that typically K decreases more slowly than τ is equivalent to their ratio increasing with height, consistent with an increase of the Richardson number (Zilitinkevich *et al.*, 2013). Furthermore, as K increases with height, h_K becomes negative and so the concept of depth has no meaning; an interpretation of these values will be given in the discussion of uSBL cases. Note that values much larger than the tower height must be considered as purely indicative extrapolations; however most of the depths are less than three times the highest instrument level, as far as the momentum and heat depths are concerned (the 90th percentiles are 89, 74 and 187 m for h_τ , h_Q and h_K respectively).

For each case, i.e. in the same time interval, the distributions of the ratios h_Q/h_τ and h_K/h_τ (for $h_K > 0$) further confirm that the SBL depths are different for different moments. The median values are 0.9 and 2.2 respectively, the 10th percentiles are 0.3 and 0.9, and the 90th percentiles 1.8 and 5.8. These values tell us that in almost 50% of the cases $h_Q > h_\tau$ (and obviously in the remaining fraction of cases $h_Q < h_\tau$), but only in 10% of cases is $h_Q > 2h_\tau$. h_K is lower than h_τ in only 10% of cases (Table 3).

A summarizing picture is made by plotting the vertical profiles of the moments, normalized with their surface values, as a function of z/h_τ (Figure 4). With this normalization, the data are represented by the non-dimensional profiles

$$\frac{y(z)}{y_0} = 1 - \alpha_{\tau y} \frac{z}{h_\tau}, \quad \alpha_{\tau y} = \frac{h_\tau}{h_y}, \quad (2)$$

where $y_0 = a$ and for the momentum profile $\alpha_{\tau\tau} = 1$ obviously, while for heat flux and turbulent kinetic energy $\alpha_{\tau y}$ changes according to the value of the ratio for each specific case. In Figure 4 the dashed line represents Eq. (2) with $\alpha_{\tau y}$ given from the median of the ratios of the corresponding depths. The solid line is the linear fit of vertically binned data.

For the momentum flux, Figure 4(a) shows that the largest spreads occur for the two lowest instruments, as the major variation of the flux occurs in the lowest layer (Figure 1(a)), and the collapse on the lines is good. For the heat flux and the turbulent kinetic energy (Figure 4(b, c)), the choice of the scale relative to the momentum flux allows us to show the different heights at which each momentum goes to negligible values (the different SBL depths) and the scatter of the depth ratios around its median value. As far as Q is concerned (Figure 4(b)), it is evident from the binned data that most of the decrease occurs in the lower half of the SBL, while in the upper part it lies between 0.3 and 0.4 of its surface value. This underlines that even in the selected cases satisfying the Eq. (1) criterion, the concave profiles are the most frequent. In a few cases, Q changes its sign at the upper measuring level, giving rise to locally unstable conditions (positive heat flux). For the cases of turbulent kinetic energy decreasing with height

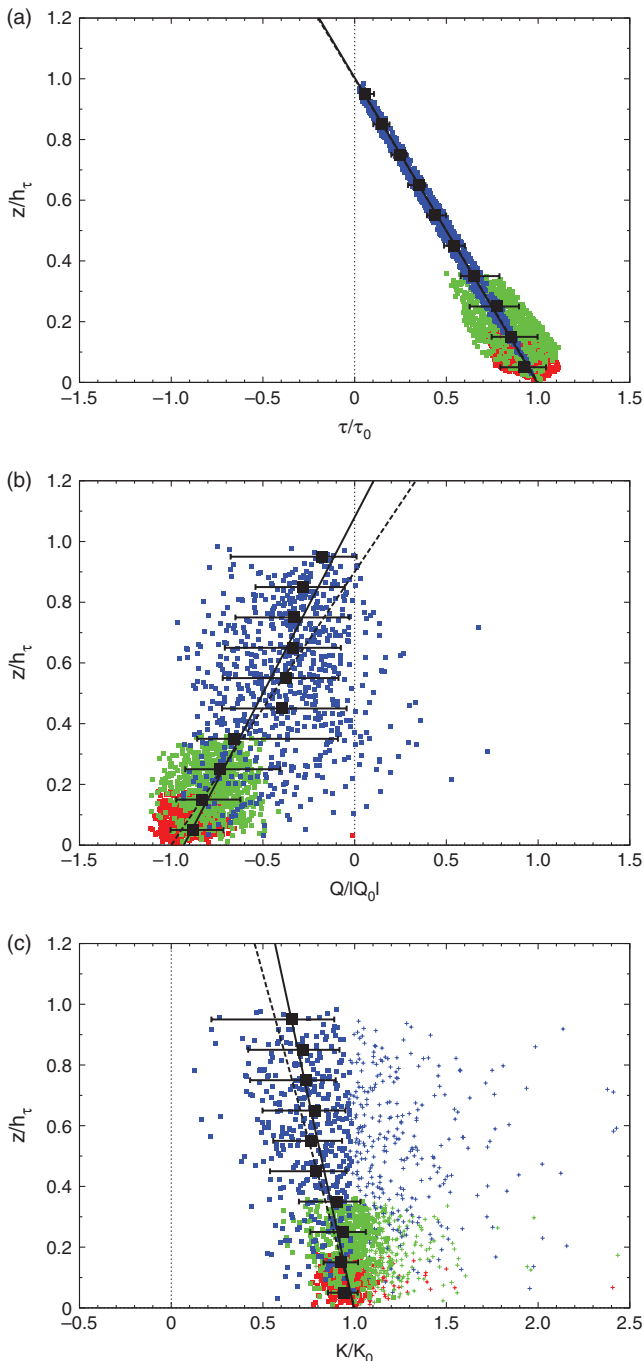


Figure 4. Non-dimensional vertical profiles of (a) the momentum flux, (b) heat flux, and (c) turbulent kinetic energy. The height is normalized with h_τ . Red symbols refer to R2 data, green symbols to R3 data, and blue symbols to CS data. Large black squares with error bars represent the median values and the 10th and 90th percentiles for bins of range $0.1 z/h_\tau$. The solid lines are fits on the medians from the binned data. The dashed lines represent Eq. (2) with the median values of the ratios h_Q/h_τ and h_K/h_τ . In (b) the heat flux is normalized with the modulus of its surface value. In (c) the crosses denote cases of turbulent kinetic energy increasing with height; binning of the data was limited to the decreasing K cases.

(Figure 4(c), full symbols) the weaker decrease with height with respect to momentum flux is confirmed.

For the traditional SBL, the depths determined from the linear fit may be compared with the equilibrium depths derived on the basis of ground-level fluxes and atmospheric stability, according for instance to the formula (Zilitinkevich and Mironov, 1996; Zilitinkevich and Esau, 2007)

$$\frac{1}{h_E^2} = \frac{f^2}{C_R^2 \tau_0} + \frac{N|f|}{C_{CN}^2 \tau_0} - \frac{|f|(g/\theta_{00})Q_0}{C_{NS}^2 \tau_0^2} \quad (3)$$

where f is the Coriolis parameter ($f = 1.4 \times 10^{-4} \text{ s}^{-1}$ at Ny-Ålesund), N the Brunt-Väisälä frequency estimated from the

mean temperatures measured at CCT, g the gravity acceleration, $\Theta(0)$ a reference mean value of potential temperature, in this case taken near the ground, and $C_R = 0.6$, $C_{CN} = 1.36$, $C_{NS} = 0.51$ (see references for the definition of these constants). The surface values for the fluxes are those obtained from the linear fits. This equation takes into account three factors: (i) rotation, (ii) stability of the lower troposphere at the SBL top and (iii) surface fluxes. We estimated the three factors independently and in most of our cases, i.e. for $h_E < 200 \text{ m}$ that occurs in 80% of the cases, the surface flux term was dominant. Above this threshold the second term becomes dominant, while the first term is always negligible. The distribution of the ratio h_E/h_τ gives a median value of 1.7, while the 25th percentile is almost 1. Thus Eq. (3) gives an estimate of the depth of tSBL which is, on average, almost twice that obtained from the linear fit of the observations of τ taken at different heights, and $h_E > h_\tau$ in 25% of cases. The ratio h_E/h_K shows a median value of 0.8 and about 50% of cases lies between 0.5 and 1.4. This suggests that Eq. (3) gives a better approximation for h_K than for h_τ (Table 3).

We also used our data to evaluate the exponents γ and δ of two formulations of the SBL depth proposed by Mironov and Fedorovich (2010) (their Eqs 16 and 17). For values of these exponents equal to $1/2$, the two formulae reduce to the third and the second term of Eq. (3). We obtained $\gamma = 1.4$ and $\gamma = 1.2$ for h_τ and h_K respectively, with correlation coefficients equal to -0.8 and -0.7 , while $\delta \approx 1$ for both the depths h_τ and h_K , but with a poor correlation (-0.4). This result outlines that the tSBL cases are more influenced by the surface fluxes than by the stabilities aloft (Mironov and Fedorovich, 2010).

3.3. Upside-down SBL

Upside-down SBLs occur as the turbulent fluctuations of velocity and temperature are produced by instabilities aloft. The natural scale should be the moment value at the production height, but it cannot be determined from the present data. Thus we decide to use as scale for τ and K the value derived from the fit at the surface, provided that it is larger than its statistical error, with the correct sign (positive for τ and K , negative for Q). As far the height is concerned, the positive scales of variation $s = a/b$ for momentum and heat fluxes (respectively indicated by s_τ and s_K) are defined. The value of s represents the height at which the considered moment becomes twice its surface value, so that it gives a measure of the rate of change with height: very large values of s would correspond to approximately constant profiles. The heat flux slope may be either positive and negative (Figure 2(a)); in the former case a depth $h_Q = -s_Q$ can be recognized.

The frequency distributions of the scales are shown in Figure 5. As for the tSBL case, the momentum and heat flux scales in the positive range present similar distributions, while that of K is more elongated toward higher values. The median values are 11.4, 17.0 and 52.1 m, respectively (Table 3).

The non-dimensional profiles can be represented in the following form:

$$\frac{y(z)}{y_0} = 1 + \beta_{\tau y} \frac{z}{s_\tau}, \quad \beta_{\tau y} = \frac{s_\tau}{s_y}, \quad (4)$$

where obviously $\beta_{\tau\tau} = 1$. As in the tSBL case, the scales in general turn out to be different for the different moments at the same time: the ratio s_Q/s_τ has a median value of 1.2, while the 10th and 90th percentiles are 0.2 and 5.5, respectively (Table 3). As for the ratio s_K/s_τ , the median value is 4.7, the 10th percentile is 0.8 and the 90th percentile 26.5 (Table 3). The non-dimensional vertical profiles of τ , Q and K according to Eq. (4) are reported in Figure 6. It appears that the heat flux normalized profile has a large spread, even considering only cases of absolute value increasing with height. Moreover, similarly to the tSBL case, the largest variation occurs in the lower part of the SBL.

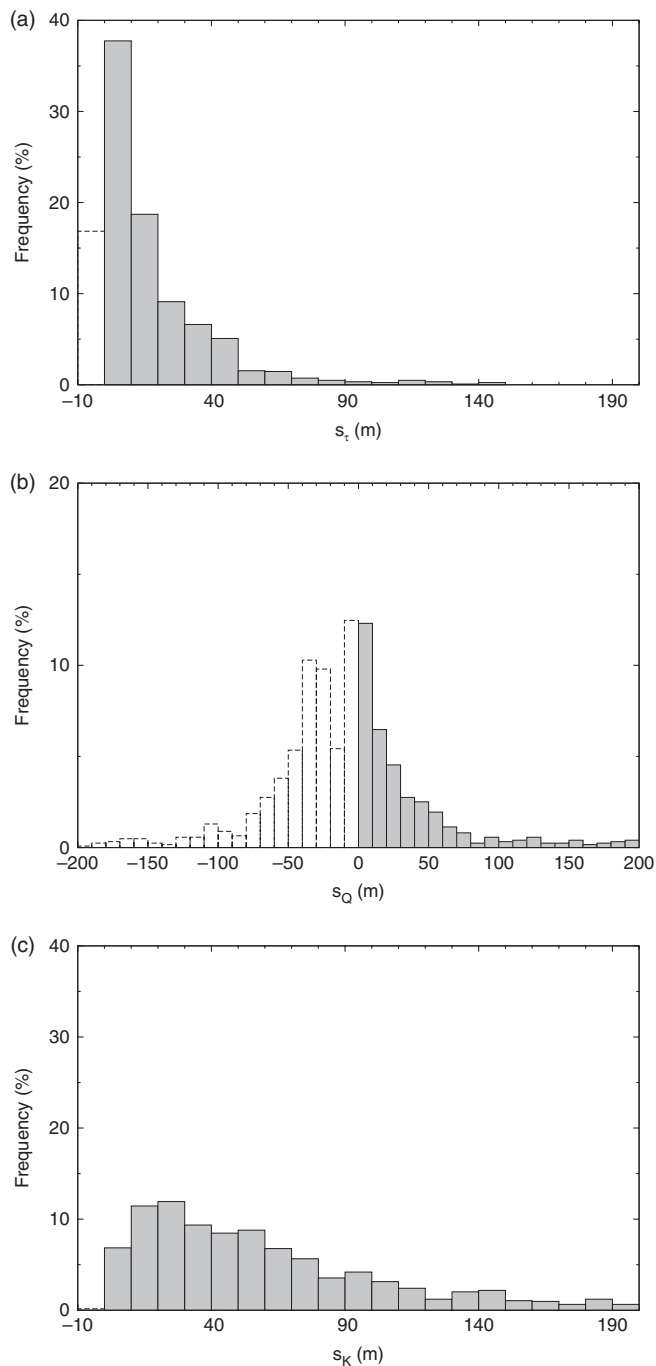


Figure 5. Frequency distributions for uSBL scales (a) s_τ , (b) s_Q , and (c) s_K .

4. The relation between vertical structure of moments and Obukhov length

To investigate the vertical profile of stability, the Obukhov length and the Richardson number can be used. As noticed by Sorbjan (2010) and Grachev *et al.* (2015), for large stability the heat flux becomes very small and the Obukhov length is an unreliable measure. The present dataset does not involve a significant number of very stable cases (see below) so that the Obukhov length can be used.

The local value of the Obukhov length Λ (Obukhov, 1946) is expressed as:

$$\Lambda(z) = -\frac{\Theta(z) \tau^{3/2}(z)}{\kappa g Q(z)}, \quad (5)$$

where $\kappa = 0.4$ the von Kármán constant.

The value of z/Λ measured by R2 shows that there is a large variability for both tSBL and uSBL cases: for the former the median is 0.023 (with 10th and 90th percentiles 0.007 and

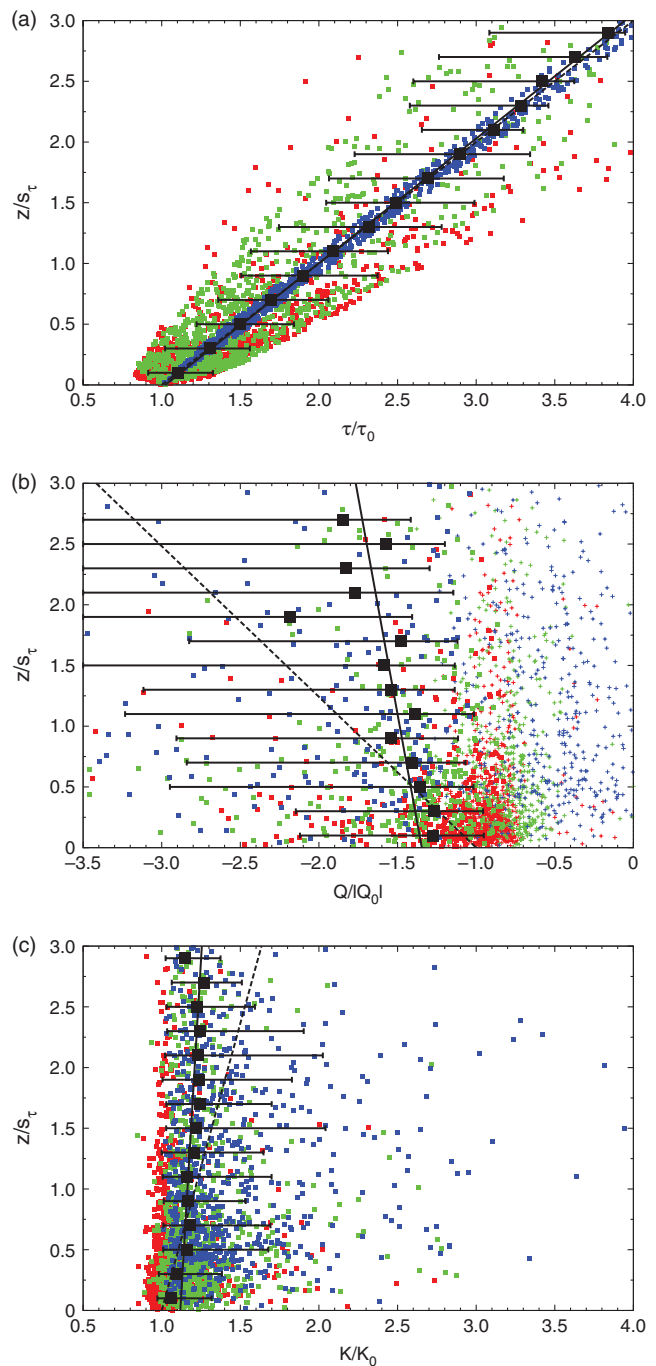


Figure 6. As Figure 4, but for uSBL. The height is normalized with s_τ . The dashed lines represent Eq. (4) with the median values of the ratios s_Q/s_τ and s_K/s_τ . In (b) the crosses denote cases of heat flux increasing with height; binning of the data was limited to the decreasing Q cases.

0.076), and for the latter the median is 0.052 (with 10th and 90th percentiles 0.008 and 0.339). Thus the tSBL and uSBL cases show moderate values of the stability at the surface and to a large extent they cover the same stability conditions, although uSBL can be considered slightly more stable than tSBL, especially as far as the right tail of the distribution is concerned (not shown).

The vertical profile of $\Lambda(z)/L$ is shown in Figure 7 for tSBL and uSBL cases. Here, L is computed from Eq. (5) using the surface values of the fluxes obtained from the linear fits. It is evident that a unique profile cannot be recognized: the spread of the data increases as the height increases towards the top of the SBL. However, selecting cases with defined value of h_Q/h_τ or s_Q/s_τ , the data show well-defined profiles. In the tSBL cases the Obukhov length diminishes with height for $h_Q > h_\tau$ (e.g. the red to grey dots in Figure 7(a)) while it increases for $h_Q < h_\tau$ and diverges at $z \simeq h_Q$ (blue to green symbols in the same figure). Similarly, in the uSBL cases the Obukhov length increases slowly

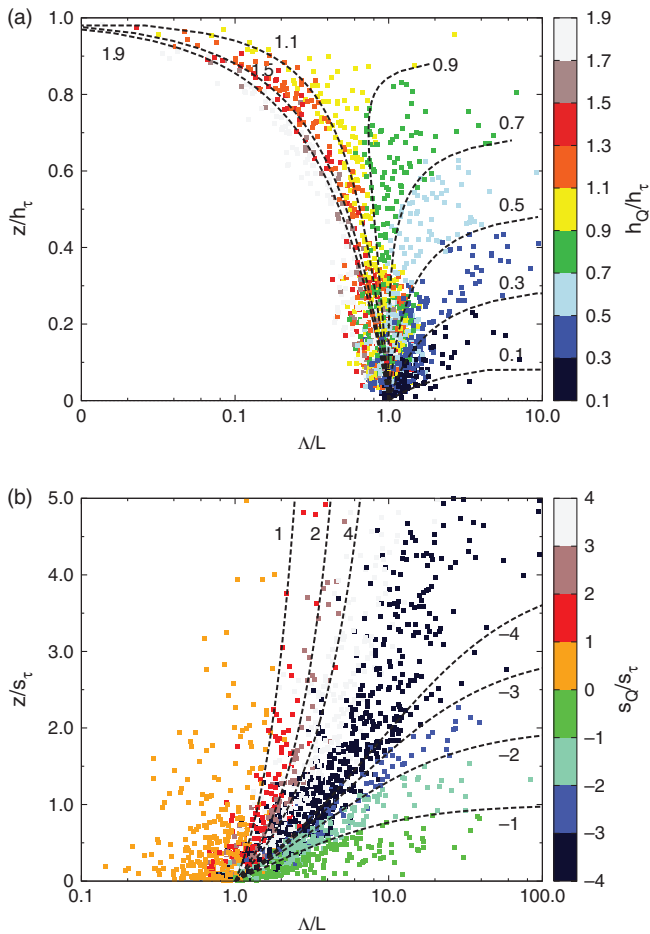


Figure 7. Vertical distributions of $\Lambda(z)/L$ for (a) tSBL and (b) uSBL cases. The height is normalized to the momentum scales h_τ and s_τ , respectively. The different colours denote ranges in the ratios of the heat flux to momentum flux scales. The dashed lines represent the theoretical curves of Eqs (6) and (7).

for $s_Q \geq s_\tau$ (red to grey symbols in Figure 7(b)) while it diverges when the sign of the heat flux scale is negative, because the heat flux goes to zero at $h_Q = -s_Q$ (blue to green symbols in the same figure).

These behaviours are consistent with the relation

$$\frac{\Lambda(z)}{L} = \frac{(1 - z/h_\tau)^{3/2}}{1 - z/h_Q}, \tag{6}$$

for tSBL, and

$$\frac{\Lambda(z)}{L} = \frac{(1 + z/s_\tau)^{3/2}}{1 + z/s_Q}, \tag{7}$$

for uSBL, derived simply by the prescribed linear shapes of τ and of Q . Equation (6) is reported for different values of h_Q/h_τ in Figure 7 (a), and Eq. (7) is reported for different values of s_Q/s_τ in Figure 7 (b). In both the cases, a fair agreement with the data results.

5. Conclusions

The analysis of 10 min averaged tower data from three sonic anemometers allowed us to investigate the instantaneous shape of the height profiles of the momentum flux, the heat flux and the turbulent kinetic energy in stable conditions. Only cases satisfying a criterion of linearity of the profiles have been selected, for two different situations: traditional SBL and upside-down SBL.

The analysis allows us to estimate the scales of variation with heights of the different moments. The three scales were found to assume different values, in particular for turbulent kinetic energy

they are larger than the others, i.e. in general the turbulent kinetic energy changes with height more slowly than the momentum flux or the heat flux.

For the traditional SBL cases, the scale heights give an estimate of the depth of the boundary layer. The depth based on K was found to be larger than that based on momentum. The equilibrium height computed from the surface fluxes according to Zilitinkevich and Esau (2005) was shown to be fairly consistent with h_K .

In the upside-down SBL cases, similar considerations apply for the s scales. In particular, as K increases with height, its scale s_K is typically larger than s_τ .

Assumed that the profiles of τ and Q are linear and characterized by different scale heights, the Obukhov length vertical profiles can be computed, and their variations with height depend on the ratio between the scales. This simple observation demonstrates that the SBL cannot be characterized by a single value of stability (e.g. the Obukhov length in the surface layer).

Moreover it must be noted that the occurrence of different scales for τ and K corresponds to a ratio τ/K which is not constant in general, but in most cases increases with height. This observation is consistent with a picture of SBL where this ratio is a function of stability (e.g. Mauritsen and Svensson, 2007) and stability increases with height (Sorbján, 2012). It must be remembered that the value of this ratio and its dependence on stability is relevant in most of the turbulence closures used in numerical models. (References to closures can be found in Cuxart *et al.*, 2006; Bosveld *et al.*, 2014).

The classification of SBLs in terms of traditional and upside-down cases has a relevance in the interpretation of observations, and thus has an impact on the verification of the numerical models and the assessment of the parametrizations adopted. Traditional SBLs are fairly well represented in numerical simulations (e.g. Beare *et al.*, 2006), since the surface fluxes are important in the dynamics of the surface layer.

Because the upside-down SBLs are driven by the production of turbulent kinetic energy aloft, and while the surface fluxes turn out to be small (in absolute value) or almost negligible, their treatment in the numerical models cannot rely too much on any closure based on surface-layer similarity theory. High vertical resolution is necessary to deal properly with the occurrence of low-level jets leading to the shear and turbulence production aloft.

As a further aspect, note that in the numerical modelling of air quality, a challenging point is the correct treatment of low-wind conditions (e.g. Wenjun and Venkatram, 2011). In the present dataset, the occurrence of low-wind conditions (less than 1 m s^{-1} at the lowest anemometer) is twice as frequent for uSBL as for tSBL, further suggesting the need for a careful simulation of near-surface conditions and treatment of the vertical profile of turbulence.

Subsequent work will investigate the applicability of profiles other than the linear one to the analysis of the SBL turbulence structure, as well as the implications of the different scale heights for the similarity relationships for first and second-order moments.

Many studies in the literature have focused on the different SBL regimes and on their transitions (Sun *et al.*, 2012; Mahr, 2014; Grachev *et al.*, 2015), noticing that the Richardson number is in general the key parameter separating fully developed turbulent layers and intermittent stable layers affected by non-local perturbations. Future research will relate the vertical profiles of statistical moments to the regimes, to give a better description of the complexities of the SBL.

Acknowledgements

This work was partly supported by the Italian Ministry of Foreign Affairs in the framework of bilateral project Italy–Korea

2013–2015 and by a National Research Foundation of Korea Grant funded by the Korean Government (MSIP) (NRF-C1ABA001-2011-0021063, PN14081). The authors wish to thank the Department of Earth System Science and Environmental Technologies of the CNR for supporting the realization of the Climate Change Tower – Integrated Project. They are also grateful to the management of the Italian Arctic station Dirigibile Italia for the technical and logistic support.

References

- Andreas EL, Fairall CW, Guest PS, Persson POG. 1999. An overview of the SHEBA atmospheric surface flux program. In *Proceedings of 13th Symposium on Boundary Layers and Turbulence*, 10–15 January 1999, Dallas, TX: 550–555. American Meteorological Society: Boston MA.
- Banta RM, Pichugina YL, Brewer WA. 2006. Turbulent velocity-variance profiles in the stable boundary layer generated by a nocturnal low-level jet. *J. Atmos. Sci.* **63**: 2700–2719.
- Beare RJ, Macvean MK, Holtslag AAM, Cuxart J, Esau IN, Golaz J-C, Jimenez MA, Khairoutdinov M, Kosovic B, Lewellen D, Lund TS, Lundquist JK, McCabe A, Moene AF, Noh Y, Raasch S, Sullivan PP. 2006. An intercomparison of large-eddy simulations of the stable boundary layer. *Boundary-Layer Meteorol.* **118**: 247–272.
- Bosveld FC, Baas P, Steeneveld GJ, Holtslag AAM, Angevine WM, Bazile E, De Bruin H, Deacu D, Edwards J, Ek M, Larson VE, Raschendorfer M, Svensson G. 2014. The third GABLS intercomparison case for evaluation studies of boundary-layer models. Part B: Results and process understanding. *Boundary-Layer Meteorol.* **152**: 157–187.
- Caughey SJ, Wyngaard JC, Kaimal JC. 1979. Turbulence in the evolving stable boundary layer. *J. Atmos. Sci.* **36**: 1041–1052.
- Cuxart J, Holtslag AAM, Beare RJ, Bazile E, Beljaars A, Cheng A, Conangla L, Ek M, Freedman F. 2006. Single-column model intercomparison for a stably stratified atmospheric boundary layer. *Boundary-Layer Meteorol.* **118**: 273–303.
- Dai C-Y, Gao Z-Q, Wang Q, Cheng G. 2011. Analysis of atmospheric boundary-layer height characteristics over the Arctic Ocean using the aircraft and GPS soundings. *Atmos. Oceanic Sci. Lett.* **4**: 124.
- Grachev AA, Fairall CW, Persson POG, Andreas EL, Guest PS. 2005. Stable boundary-layer scaling regimes: The SHEBA data. *Boundary-Layer Meteorol.* **116**: 201–235.
- Grachev AA, Andreas EL, Fairall CW, Guest PS, Persson POG. 2015. Similarity theory based on the Dougherty–Ozmidov length scale. *Q. J. R. Meteorol. Soc.* **141**: 1845–1856.
- Handorf D, Foken T, Kottmeier C. 1999. The stable atmospheric boundary layer over an Antarctic ice sheet. *Boundary-Layer Meteorol.* **91**: 165–189.
- Howell J, Mahrt L. 1997. Multiresolution flux decomposition. *Boundary-Layer Meteorol.* **83**: 117–137.
- IPCC. 2007. *Climate Change 2007 – The Physical Science Basis: Contribution of Working Group I to the Fourth Assessment Report of the Intergovernmental Panel on Climate Change*. Cambridge University Press: Cambridge, UK and New York, NY.
- IPCC. 2013. *Climate Change 2013 – The Physical Science Basis: Contribution of Working Group I to the Fifth Assessment Report of the Intergovernmental Panel on Climate Change*. Cambridge University Press: Cambridge, UK and New York, NY.
- Jocher G, Schulz A, Ritter C, Neuber R, Dethloff K, Foken T. 2015. The sensible heat flux in the course of the year at Ny-Ålesund, Svalbard: Characteristics of eddy covariance data and corresponding model results. *Adv. Meteorol.* **2015**: 852108, doi: 10.1155/1306.
- Kilpelinen T, Sjöblom A. 2010. Momentum and sensible heat exchange in an ice-free arctic fjord. *Boundary-Layer Meteorol.* **134**: 109–130.
- Kral ST, Sjöblom A, Nygrd T. 2014. Observations of summer turbulent surface fluxes in a high Arctic fjord. *Q. J. R. Meteorol. Soc.* **140**: 666–675.
- Lenschow DH, Li XS, Zhu CJ, Stankov BB. 1988. The stably stratified boundary layer over the Great Plains. *Boundary-Layer Meteorol.* **42**: 95–121.
- Mahrt L. 2014. Stably stratified atmospheric boundary layers. *Ann. Rev. Fluid Mech.* **46**: 23–45.
- Mahrt L, Vickers D. 2002. Contrasting vertical structures of nocturnal boundary layers. *Boundary-Layer Meteorol.* **105**: 351–363.
- Maturilli M, Herber A, König-Langlo G. 2013. Climatology and time series of surface meteorology in Ny-Ålesund, Svalbard. *Earth Syst. Sci. Data* **5**: 155–163.
- Mauritsen T, Svensson G. 2007. Observations of stably stratified shear-driven atmospheric turbulence at low and high Richardson numbers. *J. Atmos. Sci.* **64**: 645–655.
- Mironov DV, Fedorovich E. 2010. On the limiting effect of the Earth's rotation on the depth of a stably stratified boundary layer. *Q. J. R. Meteorol. Soc.* **136**: 1473–1480.
- Monahan AH, Rees T, He Y, McFarlane N. 2015. Multiple regimes of wind, stratification, and turbulence in the stable boundary layer. *J. Atmos. Sci.* **72**: 3178–3198.
- Nieuwstadt FTM. 1984. The turbulent structure of the stable nocturnal boundary layer. *J. Atmos. Sci.* **41**: 2202–2216.
- Obukhov AM. 1946. Turbulence in thermally inhomogeneous atmosphere. *Trudy In-ta Theor. Geofiz. AN SSSR* **1**: 95–115 (in Russian).
- Persson POG, Fairall CW, Andreas EL, Guest PS, Perovich DK. 2002. Measurements near the atmospheric surface flux group tower at SHEBA: Near-surface conditions and surface energy budget. *J. Geophys. Res.* **107**: 8045, doi: 10.1029/2000JC000705.
- Serreze MC, Barrett AP, Stroeve JC, Kindig DN, Holland MM. 2009. The emergence of surface-based Arctic amplification. *Cryosphere* **3**: 11–19.
- Sorbjan Z. 1988. Structure of the stably-stratified boundary layer during the SESAME-1979 experiment. *Boundary-Layer Meteorol.* **44**: 255–266.
- Sorbjan Z. 2010. Gradient-based scales and similarity laws in the stable boundary layer. *Q. J. R. Meteorol. Soc.* **136**: 1243–1254.
- Sorbjan Z. 2012. The height correction of similarity functions in the stable boundary layer. *Boundary-Layer Meteorol.* **142**: 21–31.
- Sorbjan Z, Czerwinska A. 2013. Statistics of turbulence in the stable boundary layer affected by gravity waves. *Boundary-Layer Meteorol.* **148**: 73–91.
- Stroeve J, Holland MM, Meier W, Scambos T, Serreze M. 2007. Arctic sea ice decline: Faster than forecast. *Geophys. Res. Lett.* **34**: L09501, doi: 10.1029/2007GL029703.
- Stroeve JC, Kattsov V, Barrett A, Serreze M, Pavlova T, Holland M, Meier WN. 2012. Trends in Arctic sea ice extent from CMIP5, CMIP3 and observations. *Geophys. Res. Lett.* **39**: L16502, doi: 10.1029/2012GL052676.
- Sun J, Mahrt L, Banta RM, Pichugina YL. 2012. Turbulence regimes and turbulence intermittency in the stable boundary layer during CASES-99. *J. Atmos. Sci.* **69**: 338–351.
- Wenjun Q, Venkatram A. 2011. Performance of steady-state dispersion models under low wind-speed conditions. *Boundary-Layer Meteorol.* **138**: 475–491.
- Zilitinkevich SS, Esau IN. 2005. Resistance and heat-transfer laws for stable and neutral planetary boundary layers: Old theory advanced and re-evaluated. *Q. J. R. Meteorol. Soc.* **131**: 1863–1892.
- Zilitinkevich SS, Esau IN. 2007. Similarity theory and calculation of turbulent fluxes at the surface for the stably stratified atmospheric boundary layer. *Boundary-Layer Meteorol.* **125**: 193–205.
- Zilitinkevich SS, Mironov DV. 1996. A multi-limit formulation for the equilibrium depth of a stably stratified boundary layer. *Boundary-Layer Meteorol.* **81**: 325–351.
- Zilitinkevich SS, Elperin T, Kleerorin N, Rogachevskii I, Esau IN. 2013. A hierarchy of energy- and flux-budget (EFB) turbulence closure models for stably-stratified geophysical flows. *Boundary-Layer Meteorol.* **146**: 341–373.